Three-Dimensional Quasi-linear Electromagnetic Modeling and Inversion

Michael S. Zhdanov
Sheng Fang

Summary. The quasi-linear (QL) approximation replaces the (unknown) total field in the integral equation of electromagnetic (EM) scattering with a linear transformation of the primary field. This transformation involves the product of the primary field with a reflectivity tensor, which is assumed to vary slowly inside inhomogeneous regions and therefore can be determined numerically on a coarse grid by a simple optimization. The QL approximation predicts EM responses accurately over a wide range of frequencies for conductivity contrasts of more than 100 to 1 between the scatterer and the background medium. It also provides a fast-forward model for 3-D EM inversion. The inversion equation is linear with respect to a modified material property tensor, which is the product of the reflectivity tensor and the anomalous conductivity. We call the (regularized) solution of this equation a *quasi-Born inversion.* The material property tensor (obtained by inversion of the data) then is used to estimate the reflectivity tensor inside the inhomogeneous region and, in turn, the anomalous conductivity. Solution of the nonlinear inverse problem thus proceeds through a set of linear equations. In practice, we accomplish this inversion through gradient minimization of a cost function that measures the error in the equations and includes a regularization term. We use synthetic experiments with plane-wave and controlled sources to demonstrate the accuracy and speed of the method.

1 Introduction

There has been great progress recently in 3-D electromagnetic (EM) modeling and inversion with both integral-equation (Eaton, 1989; Xiong, 1992; Xiong and Kirsch, 1992; Tripp and Hohmann, 1993; Xiong and Tripp, 1993; Xie and Lee, 1995) and finite-difference methods (Madden and Mackie, 1989; Newman and Alumbaugh, 1995). These "exact" methods, however, usually require too large a computational effort to allow their routine use. We have been developing a practical 3-D inversion based on a fast new method of forward modeling called the quasi-linear (QL) approximation (Zhdanov and Fang, 1996a). In the QL approximation, the anomalous field inside the

Department of Geology and Geophysics, University of Utah, Salt Lake City, UT 84112, USA.

inhomogeneous region is written as the product of the incident field and a reflectivity tensor. This tensor is assumed to be slowly varying, and therefore can be computed on a much coarser grid than the field itself. Our experience is that the QL approximation is easy to compute and very accurate. For the inverse problem, we recast the QL approximation as a linear integral equation for a modified material property tensor, which then is estimated from the data. The results are used to determine the reflectivity tensor and the anomalous conductivity.

Our method resembles inversion based on the extended Born approximation (Habashy et al., 1993; Torres-Verdín and Habashy, 1994, 1995a,b), but there are some important differences. For example, the extended Born approximation also replaces the (unknown) total field inside the scatterer with a product of the incident field and a tensor, but this scattering tensor is defined explicitly through a weighted integral of the anomalous conductivity. In the QL approximation, in contrast, the reflectivity tensor itself is determined by the solution of an optimization problem.

We develop QL inversion for 3-D EM fields using a gradient algorithm to solve a set of coupled linear inverse problems. The inversion is stabilized by Tikhonov regularization (Tikhonov and Arsenin, 1977; Zhdanov, 1993). Synthetic examples, with and without random noise, indicate that the algorithm for inverting 3-D EM data is fast and stable.

2 Approximations to EM scattering

Consider a 3-D geoelectric model with the normal (or background) complex conductivity $\tilde{\sigma}_n$ and local inhomogeneity D with conductivity $\tilde{\sigma} = \tilde{\sigma}_n + \Delta\tilde{\sigma}$. Complex conductivity includes the effect of displacement currents: $\tilde{\sigma} = \sigma - i\omega\varepsilon$, where σ and ε are electrical conductivity and dielectric permittivity. We assume that $\mu = \mu_0 = 4\pi \times 10^{-7}$ H/m, the free-space magnetic permeability. The model is excited by an EM field generated by an arbitrary source. This field is time harmonic as $e^{-i\omega t}$. The EM fields in this model can be split into normal and anomalous fields:

$$\mathbf{E} = \mathbf{E}^n + \mathbf{E}^a, \quad \mathbf{H} = \mathbf{H}^n + \mathbf{H}^a, \tag{1}$$

where the normal field is the field generated by the given sources in the model with the background distribution of conductivity $\tilde{\sigma}_n$, (i.e., in the model without the inhomogeneity) and the anomalous field is the difference between the total field and the normal field.

The anomalous field can be expressed as an integral over the excess (scattering) currents in the inhomogeneous domain D (Hohmann, 1975; Weidelt, 1975):

$$\mathbf{E}^a(\mathbf{r}_j) = \iiint_D \mathbf{G}^n(\mathbf{r}_j \mid \mathbf{r})\Delta\tilde{\sigma}(\mathbf{r})[\mathbf{E}^n(\mathbf{r}) + \mathbf{E}^a(\mathbf{r})]\, dv, \tag{2}$$

where $\mathbf{G}^n(\mathbf{r}_j \mid \mathbf{r})$ is the EM Green's tensor for the medium with the normal conductivity $\tilde{\sigma}_n$.

2.1 Born and extended Born approximations

If the anomalous field is small inside D (in comparison with the normal or incident field), then the anomalous field can be neglected inside the integral in Eq. (2), giving

the Born approximation for the scattering (Born, 1933):

$$\mathbf{E}^B(\mathbf{r}_j) = \iiint_D \underline{\mathbf{G}}^n(\mathbf{r}_j \mid \mathbf{r})\Delta\tilde{\sigma}(\mathbf{r})\mathbf{E}^n(\mathbf{r})\,dv. \tag{3}$$

This approximation, however, is not very accurate for EM scattering by the large conductivity contrasts (or large bodies) that are typical of geophysical problems. Habashy et al. (1993) and Torres-Verdín and Habashy (1994) developed the extended Born approximation, which replaces the internal field in the integral (2) not by the normal field, but by its projection onto a scattering tensor $\underline{\boldsymbol{\Gamma}}(r)$:

$$\mathbf{E}(\mathbf{r}) = \underline{\boldsymbol{\Gamma}}(\mathbf{r})\mathbf{E}^n(\mathbf{r}). \tag{4}$$

An expression for the scattering tensor is derived by rewriting Eq. (2) as an integral equation for the total field,

$$\mathbf{E}(\mathbf{r}_j) = \mathbf{E}^n(\mathbf{r}_j) + \iiint_D \underline{\mathbf{G}}^n(\mathbf{r}_j \mid \mathbf{r})\Delta\tilde{\sigma}(\mathbf{r})\mathbf{E}(\mathbf{r})\,dv, \tag{5}$$

and then approximating $\mathbf{E}(\mathbf{r})$ in the integral by its value at the point $\mathbf{r}_j$.

$$\mathbf{E}(\mathbf{r}_j) \approx \mathbf{E}^n(\mathbf{r}_j) + \mathbf{E}(\mathbf{r}_j) \iiint_D \underline{\mathbf{G}}^n(\mathbf{r}_j \mid \mathbf{r})\Delta\tilde{\sigma}(\mathbf{r})\,dv, \tag{6}$$

or

$$\mathbf{E}(\mathbf{r}_j) \approx \left[\mathbf{I} - \iiint_D \underline{\mathbf{G}}^n(\mathbf{r}_j \mid \mathbf{r})\Delta\tilde{\sigma}(\mathbf{r})\,dv\right]^{-1} \mathbf{E}^n(\mathbf{r}_j). \tag{7}$$

The expression in brackets is the scattering tensor; it does not depend on the illuminating sources and is an explicit nonlinear functional of the anomalous conductivity. In forward modeling with the extended Born approximation, the scattering tensor can be calculated directly; in inversion, the scattering tensor is calculated for an (assumed) initial model, and then updated iteratively after solving an inverse problem for the anomalous conductivity. Torres-Verdín and Habashy (1994) also showed that, for some models, the iterative procedure could be collapsed into a simple two-step inversion.

2.2 QL approximation

In Zhdanov and Fang (1996a), we developed ideas that can be considered an extension of Torres-Verdín and Habashy's (1994) method. Expression (2) can be rewritten in operator form:

$$\mathbf{E}^a = \mathbf{C}[\mathbf{E}^a], \tag{8}$$

where $\mathbf{C}[\mathbf{E}^a]$ is an integral operator on the anomalous field $\mathbf{E}^a$:

$$\mathbf{C}[\mathbf{E}^a] = \mathbf{A}[\mathbf{E}^n] + \mathbf{A}[\mathbf{E}^a], \tag{9}$$

and $\mathbf{A}$ is a linear scattering operator:

$$\mathbf{A}[\mathbf{E}] = \iiint_D \underline{\mathbf{G}}^n(\mathbf{r}_j \mid \mathbf{r})\Delta\tilde{\sigma}(\mathbf{r})\mathbf{E}(\mathbf{r})\,dv. \tag{10}$$

The solution of the integral equation (8) for the anomalous field $\mathbf{E}^a$ is a fixed point of the operator $\mathbf{C}$. This solution therefore can be obtained by the method of successive iterations,

$$\mathbf{E}^{a(N)} = \mathbf{C}\left[\mathbf{E}^{a(N-1)}\right], \quad N = 1, 2, 3 \ldots, \tag{11}$$

which converges if $\mathbf{C}$ is a contraction operator; that is, if $\|\mathbf{C}\| < 1$.

The Born approximation is simply the first iteration of this scheme when the initial approximation $\mathbf{E}^{a(0)}$ is set to zero,

$$\mathbf{E}^B = \mathbf{E}^{a(1)} = \mathbf{C}[0] = \mathbf{A}[\mathbf{E}^n]. \tag{12}$$

We try to obtain a more accurate approximation by assuming that the anomalous field inside the inhomogeneous domain is linearly related to the normal field by a tensor $\underset{\sim}{\lambda}$, which we call an *electrical reflectivity tensor:*

$$\mathbf{E}^a(\mathbf{r}) \approx \underset{\sim}{\lambda}(\mathbf{r})\mathbf{E}^n(\mathbf{r}). \tag{13}$$

If expression (13) is taken as the zeroth-order approximation for the scattered field inside the inhomogeneity $[\mathbf{E}^{a(0)} = \underset{\sim}{\lambda}\mathbf{E}^n]$, then the first-order approximation is

$$\mathbf{E}^{a(1)} = \mathbf{C}[\underset{\sim}{\lambda}\mathbf{E}^n] = \mathbf{A}[\mathbf{E}^n + \underset{\sim}{\lambda}\mathbf{E}^n] = \mathbf{A}[(\underset{\sim}{\mathbf{I}} + \underset{\sim}{\lambda})\mathbf{E}^n] = \mathbf{E}^a_{q\ell}. \tag{14}$$

We call this a *QL approximation* $\mathbf{E}^a_{q\ell}$ for the anomalous field. Written out explicitly, the approximation is

$$\mathbf{E}^a_{q\ell} \approx \mathbf{A}[(\mathbf{I} + \underset{\sim}{\lambda})\mathbf{E}^n] = \iiint_V \underset{\sim}{\mathbf{G}}^n(\mathbf{r}_j \mid \mathbf{r})\Delta\tilde{\sigma}(\mathbf{r})[\underset{\sim}{\mathbf{I}} + \underset{\sim}{\lambda}(\mathbf{r})]\mathbf{E}^n(\mathbf{r})\, dv. \tag{15}$$

The accuracy of the QL approximation obviously depends on the accuracy of the representation (13). The actual anomalous field $\mathbf{E}^a$ is equal to

$$\mathbf{E}^a = \mathbf{A}[\mathbf{E}^n] + \mathbf{A}[\mathbf{E}^a] \tag{16}$$

The error is therefore

$$\left\|\mathbf{E}^a - \mathbf{E}^a_{q\ell}\right\| = \|\mathbf{A}(\mathbf{E}^a - \underset{\sim}{\lambda}\mathbf{E}^n)\| \leq \|\mathbf{A}\|\|\mathbf{E}^a - \underset{\sim}{\lambda}\mathbf{E}^n\| \tag{17}$$

or,

$$\left\|\mathbf{E}^a - \mathbf{E}^a_{q\ell}\right\| \leq \|\mathbf{A}\|\varepsilon, \tag{18}$$

where $\varepsilon = \|\mathbf{E}^a - \underset{\sim}{\lambda}\mathbf{E}^n\|$, and $\|....\|$ is an L_2 norm. If the electrical reflectivity tensor $\underset{\sim}{\lambda}(\mathbf{r})$ is allowed to be a general function of $\mathbf{r}$, it is clear that ε can be made arbitrarily small. In fact, the error is zero if the reflectivity tensor is taken as the normalized dyadic product

$$\underset{\sim}{\lambda}(\mathbf{r}) = [\mathbf{E}^{n*}(\mathbf{r}) \cdot \mathbf{E}^n(\mathbf{r})]^{-1}\mathbf{E}^a(\mathbf{r})\mathbf{E}^{n*}(\mathbf{r}),$$

where the center dot is the (real) inner product $\mathbf{a} \cdot \mathbf{b} = \sum_i a_i b_i$ and the asterisk indicates complex conjugate. Of course, this expression is not very useful in practice because it involves the unknown total field.

Zhdanov and Fang (1996a) analyze different methods of determining an optimal $\underline{\lambda}$. They show that one can use the following condition to determine $\underline{\lambda}$:

$$\left\| \underline{\lambda}(\mathbf{r}_j)\mathbf{E}^n(\mathbf{r}_j) - \iiint_D \underline{\mathbf{G}}^n(\mathbf{r}_j \mid \mathbf{r})\Delta\tilde{\sigma}(\mathbf{r})[(\underline{\mathbf{I}} + \underline{\lambda})\mathbf{E}^n(\mathbf{r})]\,dv \right\| = \varphi(\underline{\lambda}) = \min! \quad (19)$$

In numerical calculations we usually asume that $\underline{\lambda}(\mathbf{r})$ is a slowly varying (tensor) function inside the anomalous domain D (the simplest form is a constant). Equation (19) then can be treated as an overdetermined problem and solved numerically by a least-squares method (Zhdanov and Fang, 1996a). After the $\underline{\lambda}$ is found, the QL approximation to the field is calculated using

$$\mathbf{F}^a \approx \iiint_D \underline{\mathbf{G}}^F(\mathbf{r}_j \mid \mathbf{r})\Delta\tilde{\sigma}(\mathbf{r})[\underline{\mathbf{I}} + \underline{\lambda}(\mathbf{r})]\mathbf{E}^n(\mathbf{r})\,dv. \quad (20)$$

where $\mathbf{F}^a$ stands for the anomalous electric ($\mathbf{E}^a$) or magnetic ($\mathbf{H}^a$) field observed outside the scatterer (e.g., at surface of the Earth), and $\underline{\mathbf{G}}^F$ is the appropriate (electric or magnetic) Green's function.

2.3 Comparison

In their roles relating unknown anomalous or total fields to the incident field, the electrical reflectivity tensor $\underline{\lambda}$ of the QL approximation and the scattering tensor $\underline{\Gamma}$ of the extended Born approximation are themselves related by the simple formula:

$$\underline{\lambda} = \underline{\Gamma} - \underline{\mathbf{I}}. \quad (21)$$

The two approximations differ significantly, however, in computing these tensors. The scattering tensor $\underline{\Gamma}$ is defined explicitly by expression (7). The accuracy of the extended Born approximation depends on how well the integral in Eq. (5) is approximated by taking the constant value for the field $\mathbf{E}(\mathbf{r}_j)$. Because the Green's dyadic is strongly peaked for values $\mathbf{r} \approx \mathbf{r}_j$, the approximation should be good if the field itself is not varying rapidly at $\mathbf{r}_j$. Habashy et al. (1993) called this the "localized approximation."

The QL approximation determines the electrical reflectivity tensor by solving a minimization problem (Eq. 19) on a coarse grid. The accuracy of QL approximation depends only on the accuracy of this discretization of $\underline{\lambda}$ and, in principle, can be made arbitrarily good, though care may be needed with a fine discretization, because Eq. (19) can become underdetermined.

3 Numerical examples of the QL approximation

This section compares the fields obtained by solving the integral equation (2) numerically, by computing the Born approximation (3), and by computing the QL approximation (15). Figure 1 shows the 3-D geoelectrical model, which consists of a homogeneous half-space of resistivity 100 ohm-m and a conductive rectangular inclusion with resistivity 1 ohm-m. The EM field in the model is excited by a horizontal rectangular loop, which is 10 × 10 m, carries a current of 1 A, and is 50 m to the left of the model. We have used the full integral-equation (IE) code, SYSEM (Xiong, 1992), and QL code, SYSEMQL (Zhdanov and Fang, 1996a) for computing the frequency-domain response of the complex conductivity structure along profiles parallel to the x-axis.

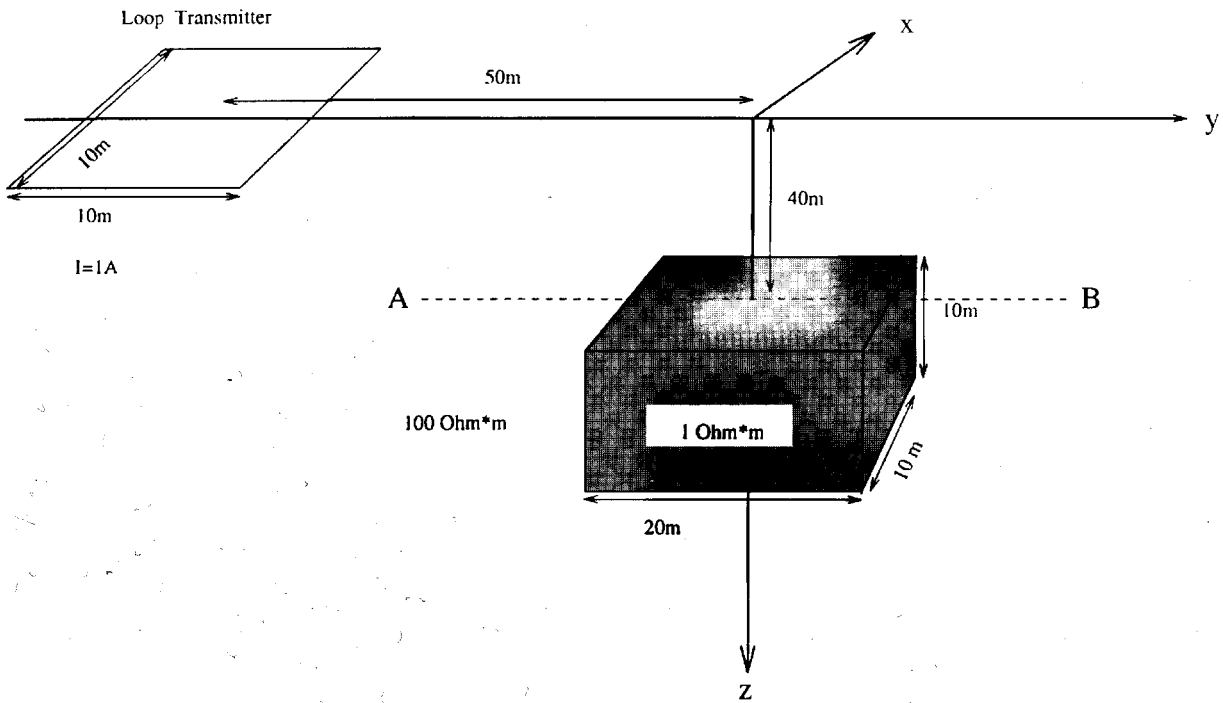

Figure 1. Three-dimensional geoelectric model, containing one conductive body in a homogeneous half-space, with rectangular loop excitation (Model 1).

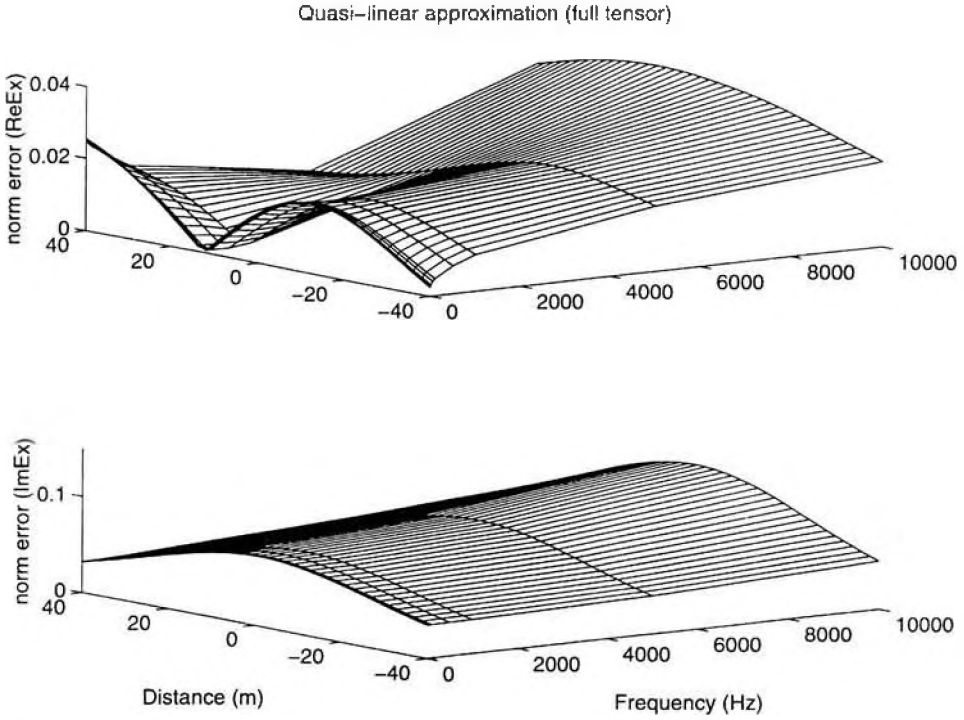

Figure 2. Numerical comparison of full IE solution and QL approximation computed for Model 1 (Fig. 1) at the frequency range from 0.1 Hz to 10 kHz. Calculations were performed for the receivers located along profiles parallel to the y-axis on the surface. Plots show the differences between IE solution and QL approximation for x-component of the secondary electric field normalized by the value of corresponding component of the field at the point $y = 40$ (normalized error).

Figures 2 and 3 compare the different solutions for real and imaginary parts of the anomalous electrical field $\mathbf{E}_x^a$ for different frequencies. The point $x = 0$ along each profile corresponds to the location of the conductive rectangular inclusion center. Figure 2 shows the differences between IE solution and QL approximation, normalized by the value of the corresponding component of the field at the point $y = 40$. The accuracy of the QL approximation for the electric-field components is within 5% for frequencies from 0.1 Hz to 10 kHz. Figure 3 presents the differences between the IE solution and Born approximation, normalized by the value of the corresponding component of the field at the point $y = 40$. The QL approximation produces a reasonable result, whereas the conventional Born approximation is far off the mark.

The next set of comparisons uses the same geometric model, but varies the body's conductivity. We selected four different resistivities of the inclusion: 1 ohm-m, 0.1 ohm-m, 0.01 ohm-m, and 0.001 ohm-m. Figure 4 shows the differences between the IE solution and the QL approximation, at a frequency 0.1 Hz, normalized by the value of the corresponding component of the field at the point $y = 40$. One of the horizontal axes on Fig. 4 is the resistivity contrast $C = \rho_i/\rho_b$, where $\rho_b = 100$ ohm-m is the resistivity of the background, and ρ_i is the resistivity of the conductive inclusion. The errors of QL approximation are generally small and grow only for very-high-conductivity contrasts, equal to $1/C = 10^5$, reaching about 10% in extremum point for the electric field. For lower-conductivity contrasts, the relative errors are below 5%.

Table 1. Comparison of CPU time (s) for the frequency-domain EM modeling, using different methods

Method	Cells in anomalous domain		
	250 cells	400 cells	800 cells
Full IE solution	1029.1	2995.0	13127.0
QL approximation	382.4	530.4	1170.1

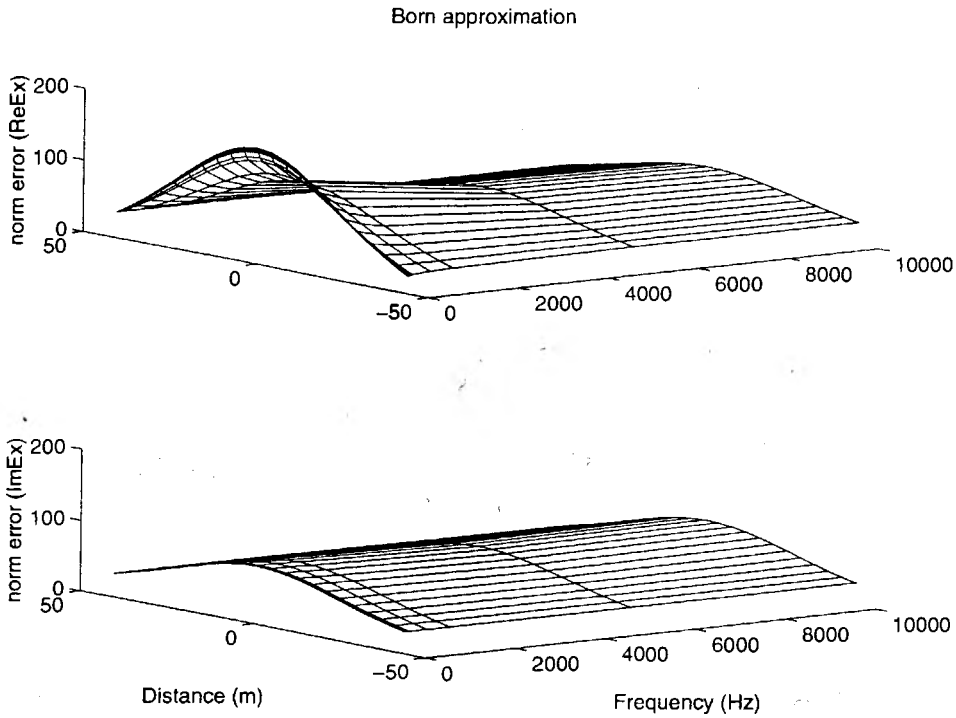

Figure 3. Numerical comparison of full IE solution and Born approximation computed for Model 1 (Fig. 1) at the frequency range from 0.1 Hz to 10 kHz. Calculations were performed for the receivers located along profiles parallel to the y-axis on the surface. Plots show the differences between IE solution and Born approximation for x-component of secondary electric field normalized by the value of corresponding component of the field at the point $y = 40$ (normalized error).

Table 1 shows the computation times needed for full IE solution and for QL approximation in the frequency domain. One can see from this table that the CPU time required for QL approximation grows much more slowly with the number of cells, than the CPU time required for the full IE solution.

4 QL inversion

For the inverse problem, we introduce a new tensor function,

$$\underline{\mathbf{m}}(\mathbf{r}) = \Delta\tilde{\sigma}(\mathbf{r})[\underline{\mathbf{I}} + \underline{\boldsymbol{\lambda}}(\mathbf{r})], \tag{22}$$

which we call a *modified material property tensor*. Equation (20) then takes the form

$$\mathbf{F}^a(\mathbf{r}_j) \approx \iiint_D \underline{\mathbf{G}}^F(\mathbf{r}_j \mid \mathbf{r})\underline{\mathbf{m}}(\mathbf{r})\mathbf{E}^n(\mathbf{r})\,dv, \tag{23}$$

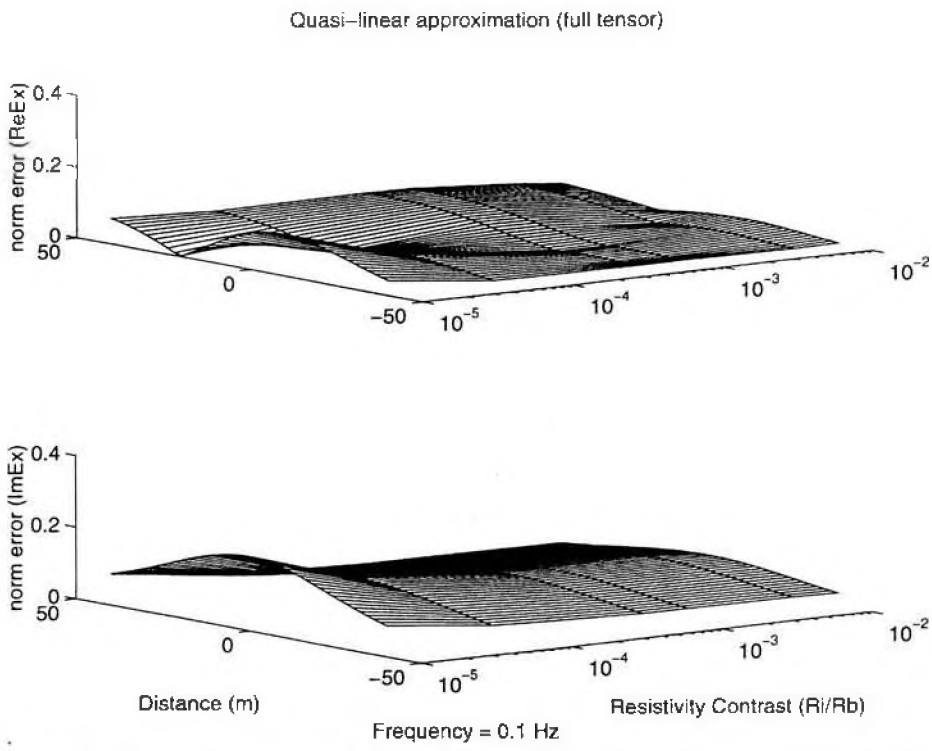

Figure 4. Numerical comparison of full IE solution and QL approximation computed for Model 1 (Fig. 1) at the resistivity ratio of inclusive body to the background range from 0.00001 to 0.01 (or -5 to -2 in log scale). Calculations were performed for the receivers located along profiles parallel to the y-axis on the surface. Plots show the differences between IE solution and QL approximation for x-component of the secondary electric field at the frequency 0.1 Hz normalized by the value of corresponding component of the field at the point $y = 40$ (normalized error).

which is linear with respect to $\underline{\mathbf{m}}(\mathbf{r})$ (the original Eq. 20 is nonlinear with respect to $\Delta\tilde{\sigma}$ because the reflectivity tensor depends implicity on $\Delta\tilde{\sigma}$). It has the same structure as the Born approximation for the anomalous field, with the modified material property tensor $\underline{\mathbf{m}}(\mathbf{r})$ replacing the anomalous conductivity $\Delta\tilde{\sigma}(\mathbf{r})$. We call Eq. (23) a *quasi-Born approximation*, and its solution (for $\underline{\mathbf{m}}$), a *quasi-Born inversion.*

The reflectivity tensor $\underline{\boldsymbol{\lambda}}$ can be computed from $\underline{\mathbf{m}}$, because

$$\mathbf{E}^a(\mathbf{r}_j) \approx \iiint_D \underline{\mathbf{G}}^E(\mathbf{r}_j \mid \mathbf{r})\underline{\mathbf{m}}(\mathbf{r})\mathbf{E}^n(\mathbf{r})\,dv \approx \underline{\boldsymbol{\lambda}}(\mathbf{r}_j)\mathbf{E}^n(\mathbf{r}_j). \tag{24}$$

Once $\underline{\mathbf{m}}$ and $\underline{\boldsymbol{\lambda}}$ are known, the anomalous conductivity $\Delta\tilde{\sigma}$ follows from Eq. (22). This inversion scheme reduces the original nonlinear inverse problem to three linear steps:

- inversion of the quasi-Born equation (23) for $\underline{\mathbf{m}}$;
- computation of the integral (24) to obtain $\underline{\boldsymbol{\lambda}}$; and
- (local) inversion of Eq. (22) to obtain the conductivity $\Delta\tilde{\sigma}$.

We call this procedure a *QL inversion.* As we explain further below, these three steps *do not* solve the full nonlinear inverse problem for $\Delta\tilde{\sigma}$ (mainly because the inversion in the first step is intrinsically nonunique), but they do provide the basis for an effective iterative solution. This iterative scheme resembles the source-type IE method of Habashy et al. (1994) and the modified gradient method of Kleinman and van den Berg (1993).

4.1 Discrete QL equations

The first step of the three-step QL inversion—the solution of Eq. (23)—is nonunique. The equation has a null space, because there exist $\mathbf{m}$ distributions that produce a zero external field, similar to the nonradiating current distributions that generate zero field outside their domain of support (Habashy et al., 1994; Svetov and Gubatenko, 1985). Although the linear inverse (source) problem for $\mathbf{m}$ is nonunique, the nonlinear inverse problem for the conductivity can be unique in the class of piecewise-analytic functions (for certain experimental configurations), according to a theorem of Gusarov (1981).

To make our QL inversion unique, we therefore have to develop a unified (iterative) approach for simultaneously finding $\mathbf{m}$, $\boldsymbol{\lambda}$, and $\Delta\tilde{\sigma}(\mathbf{r})$. We do this with a constrained inversion that generalizes a method developed by Zhdanov and Chernyak (1987) for two-dimensional (2-D) models. A similar approach to the 2-D inverse scattering problem was discussed by Kleinman and van den Berg (1993). We first discretize the equations by dividing the domain D into substructures (subdomains) $D = \bigcup_{k=1,K} D_k$ and assume that the material property tensor is constant in each substructure, so that Eq. (22) becomes

$$\mathbf{F}^a(\mathbf{r}_j) = \sum_{k=1,N} \iiint_{D_k} \mathbf{G}^F(\mathbf{r}_j \mid \mathbf{r})\mathbf{m}_k\mathbf{E}^n(\mathbf{r})\,dv. \tag{25}$$

where $\mathbf{m}_k$ depends only on k. We also assume that the reflectivity tensor is constant in each substructure so that the equation for determining $\boldsymbol{\lambda}$ is

$$\boldsymbol{\lambda}_k\mathbf{E}^n(\mathbf{r}_j) \approx \sum_{\ell=1,N} \iiint_{D_\ell} \mathbf{G}^E(\mathbf{r}_j \mid \mathbf{r})\mathbf{m}_\ell\mathbf{E}^n(\mathbf{r})\,dv, \quad \mathbf{r}_j \in D_k. \tag{26}$$

Finally,

$$\mathbf{m}_k = \Delta\tilde{\sigma}_k[\mathbf{I} + \boldsymbol{\lambda}_k] \tag{27}$$

gives the relationship between the conductivity and the material property and reflectivity tensors in each substructure.

To proceed further, we write these equations in matrix form, for the simplest case when the modified material property and reflectivity tensors are scalars (i.e., proportional to the unit tensor). Let $\mathbf{m} = [m_1, m_2, \ldots, m_N]^T$ and $\Delta\boldsymbol{\sigma} = [\Delta\tilde{\sigma}_1, \Delta\tilde{\sigma}_2, \ldots, \Delta\tilde{\sigma}_N]^T$ be column vectors whose elements are the modified material properties and conductivities in the substructures; and let $\boldsymbol{\Lambda} = \text{diag}[\lambda_1, \lambda_2, \ldots, \lambda_N]$ be a diagonal matrix of the reflectivities. Equation (25) becomes

$$\mathbf{F} = \mathbf{G}^F\mathbf{m}, \tag{28}$$

where $\mathbf{F}$ is a column vector of data, and $\mathbf{G}^F$ is a matrix representation of the linear operator defined by formula (25). Equation (27) becomes

$$\mathbf{m} = (\mathbf{I} + \boldsymbol{\Lambda})\Delta\boldsymbol{\sigma}. \tag{29}$$

This equation is essentially Ohm's law,

$$\mathbf{j}^D = \Delta\tilde{\sigma}\mathbf{E} = \Delta\tilde{\sigma}(\mathbf{E}^n + \mathbf{E}^a) = \Delta\tilde{\sigma}[\mathbf{I} + \boldsymbol{\lambda}^k(\mathbf{r})]\mathbf{E}^n. \tag{30}$$

Equation (26) is overdetermined and can be inverted directly (in least-squares sense) by

$$\lambda_k = [\mathbf{E}^{n*}(\mathbf{r}_j)\cdot\mathbf{E}^{n}(\mathbf{r}_j)]^{-1}\mathbf{E}^{n*}(\mathbf{r}_j)\cdot\sum_{\ell=1,N}\iiint_{D_\ell}\mathbf{G}^{E}(\mathbf{r}_j\mid\mathbf{r})m_\ell\mathbf{E}^{n}(\mathbf{r})\,dv,\quad \mathbf{r}_j\in D_k, \tag{31}$$

or, in matrix form,

$$\boldsymbol{\lambda} = (\underline{\mathbf{E}}^{n*}\underline{\mathbf{E}}^{n})^{-1}\underline{\mathbf{E}}^{n*}\underline{\mathbf{G}}^{E}\mathbf{m}, \tag{32}$$

where $\boldsymbol{\lambda}$ is now a column vector of the reflectivities; $\underline{\mathbf{E}}^{n}$ is a block diagonal matrix whose diagonal blocks are the (3×1 complex) vectors $\mathbf{E}^{n}(\mathbf{r}_j)$; and the asterisk indicates conjugate transpose.

With multifrequency data, both $\mathbf{m}$ and $\boldsymbol{\lambda}$ will depend on frequency. We assume, however, that $\Delta\tilde{\sigma} = \Delta\sigma - i\omega\Delta\varepsilon$, where $\Delta\sigma$ and $\Delta\varepsilon$ do not depend on frequency. In the absence of any constraints, the least-squares solution of Eq. (29) for the real and imaginary parts of $\Delta\sigma$ is

$$\mathrm{Re}(\Delta\sigma) = \mathrm{Re}\left\{\left[\sum_{\omega}(\underline{\mathbf{I}}+\underline{\boldsymbol{\Lambda}})^{*}(\underline{\mathbf{I}}+\underline{\boldsymbol{\Lambda}})\right]^{-1}\sum_{\omega}(\underline{\mathbf{I}}+\underline{\boldsymbol{\Lambda}})^{*}\mathbf{m}\right\}, \tag{33}$$

and

$$\mathrm{Im}(\Delta\sigma) = \omega\,\mathrm{Im}\left\{\left[\sum_{\omega}\omega(\underline{\mathbf{I}}+\underline{\boldsymbol{\Lambda}})^{*}(\underline{\mathbf{I}}+\underline{\boldsymbol{\Lambda}})\right]^{-1}\sum_{\omega}(\underline{\mathbf{I}}+\underline{\boldsymbol{\Lambda}})^{*}\mathbf{m}\right\}. \tag{34}$$

4.2 Regularized QL inversion

QL inversion requires the solution of Eq. (28) for $\mathbf{m}$, computation of λ_k by Eq. (31), and solution of Eq. (29) for $\Delta\tilde{\sigma}_j$. To obtain a stable, regularized solution, we introduce the functional

$$P^{\alpha}(\mathbf{m}) = \phi(\mathbf{m}) + \alpha S(\mathbf{m}), \tag{35}$$

where the misfit functional is specified as

$$\begin{aligned}\phi(\mathbf{m}) &= \|\underline{\mathbf{G}}^{F}\mathbf{m}-\mathbf{F}\|^2 + \|\mathbf{m}-(\underline{\mathbf{I}}+\underline{\boldsymbol{\Lambda}})\Delta\boldsymbol{\sigma}\|^2\\ &= (\underline{\mathbf{G}}^{F}\mathbf{m}-\mathbf{F})^{*}(\underline{\mathbf{G}}^{F}\mathbf{m}-\mathbf{F}) + [\mathbf{m}-(\underline{\mathbf{I}}+\underline{\boldsymbol{\Lambda}})\Delta\boldsymbol{\sigma}]^{*}[\mathbf{m}-(\underline{\mathbf{I}}+\underline{\boldsymbol{\Lambda}})\Delta\boldsymbol{\sigma}].\end{aligned} \tag{36}$$

The misfit functional tracks the solution of both equations (28) and (29). The stabilizer is

$$S(\mathbf{m}) = \|\mathbf{m}-\mathbf{m}_p\|^2 = (\mathbf{m}-\mathbf{m}_p)^{*}(\mathbf{m}-\mathbf{m}_p). \tag{37}$$

The prior model $\mathbf{m}_p$ is some reference model, selected on the basis of all available geological and geophysical information about the area under investigation. The scalar multiplier α is a regularization parameter.

The misfit functional provides the solution that best fits the observed data $\mathbf{F}$, whereas the stabilizing functional ties the solution to the prior model $\mathbf{m}_p$. The regularization parameter α controls the trade-off between these two goals. Principles for determining the regularization parameter α are discussed by Tikhonov and Arsenin (1977) and Zhdanov and Keller (1994). We use a simple numerical method to determine the parameter α. Consider the progression of numbers

$$\alpha_k = \alpha_0 q^{k};\quad k = 0, 1, 2, \ldots, n;\quad q > 0. \tag{38}$$

For any number α_k, we can find an element m_{α_k}, minimizing $P^{\alpha_k}(\mathbf{m})$, and calculate the misfit $\|\mathbf{G}^F\,\mathbf{m}^{\alpha_k} - \mathbf{F}\|^2$. The optimal value of the parameter α is the number α_{k0}, for which

$$\|\mathbf{G}^F\mathbf{m}^{\alpha_{k0}} - \mathbf{F}\|^2 = \delta, \tag{39}$$

where δ is the level of noise in observed data. The equality (39) is called the misfit condition. To avoid divergence, we begin an iteration from a big value of α (e.g. $\alpha_0 = 100$), then reduce α ($\alpha = \alpha_0/10$) on each subsequent iteration and continuously iterate until the misfit condition is reached.

The inversion thus is reduced to the solution of the minimization problem for the parametric functional,

$$P^{\alpha}(\mathbf{m}) = \min! \tag{40}$$

which we do by a regularized steepest-descent method (Appendix). The solution m^{α} of the regularized problem (40) is a continuous function of the data (and so, it is stable) and uniformly tends to the actual solution of the original inverse problem when $\alpha \to 0$.

5 Examples of QL inversion

5.1 *Plane-wave excitation model*

To test the algorithm, we have computed an EM field for two conductive rectangular structures in a homogeneous half-space, excited by a plane wave (Fig. 5a). The observed data on the surface were simulated by forward modeling using a full IE code (Xiong, 1992). Figures 6a and 6b show the comparison of the full IE solutions (solid line) and QL approximation (dashed line) for apparent resistivities computed for TM on (Transverse Magnetic) mode (ρ_{yx}) at the frequencies (in Hz): 10, 1, 0.5, and 0.2. Calculations are performed for the receivers at the surface located along profiles parallel to the y-axis. Figures 7a and 7b present the amplitude and the phase of the apparent resistivity distribution, calculated from the observed EM field on the surface of the Earth for the frequency equal to 1 Hz. The inversion used EM data collected along 15 profiles on the surface of the Earth at the four frequencies listed above. Displacement currents at these frequencies are negligibly smaller than the conductive currents, and so the inversion was applied only for the conductivity distribution. In the numerical test, we selected 144 substructures for inversion, shown in Fig. 5b, and we used the additional simplification that the reflectivity tensor $\hat{\boldsymbol{\lambda}}$ is scalar and constant within every substructure. The results of inversion for the data with 5% random noise added are shown on the following figures.

Figure 8 presents a vertical slice along the line $x = 0$ of the results of inversion of the noisy data. One can see clearly the cross-sections of conductive body on this picture; however, the upper part of the body is resolved slightly better than the deeper parts, which can be explained by the fact that EM field is less sensitive to the lower parts of anomalous structures. Figure 9 shows the vertical slice along the line $x = 300$ m that passes outside the body with anomalous conductivity. We can see now only background conductivity on this cross-section with a very weak variation, which corresponds very well to the original model. Figure 10 presents the volume image of the inverted model. The result clearly shows the anomalous body. The relationship between the misfit functional and the number of iterations is shown in Fig. 11. One can see that the noise practically didn't affect the result. This can be explained simply by using a regularized solution.

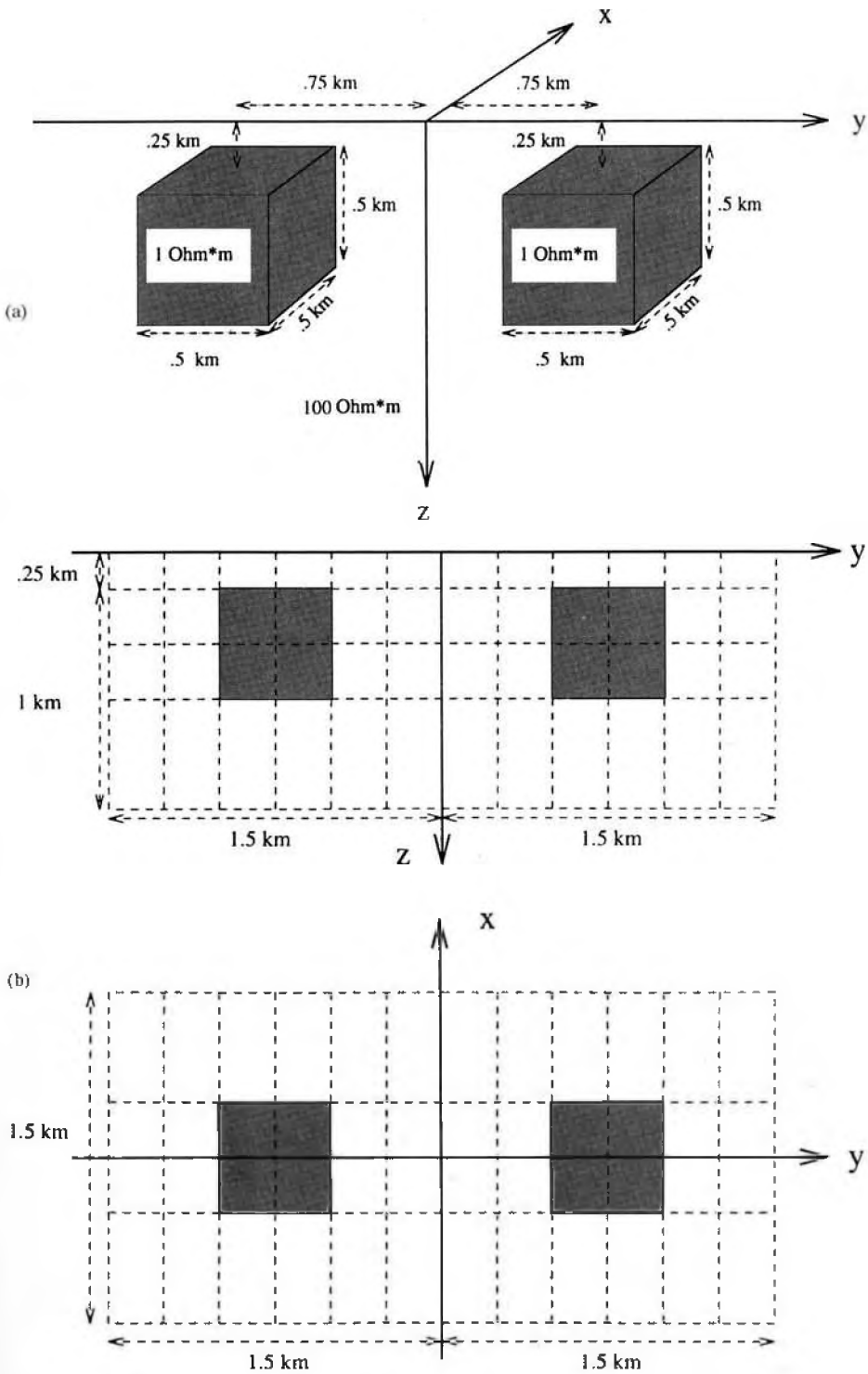

Figure 5. (a) Three-dimensional model of two rectangular conductive structures in a homogeneous half-space, excited by a plane wave (Model 2); (b) division of model into substructures used for inversion.

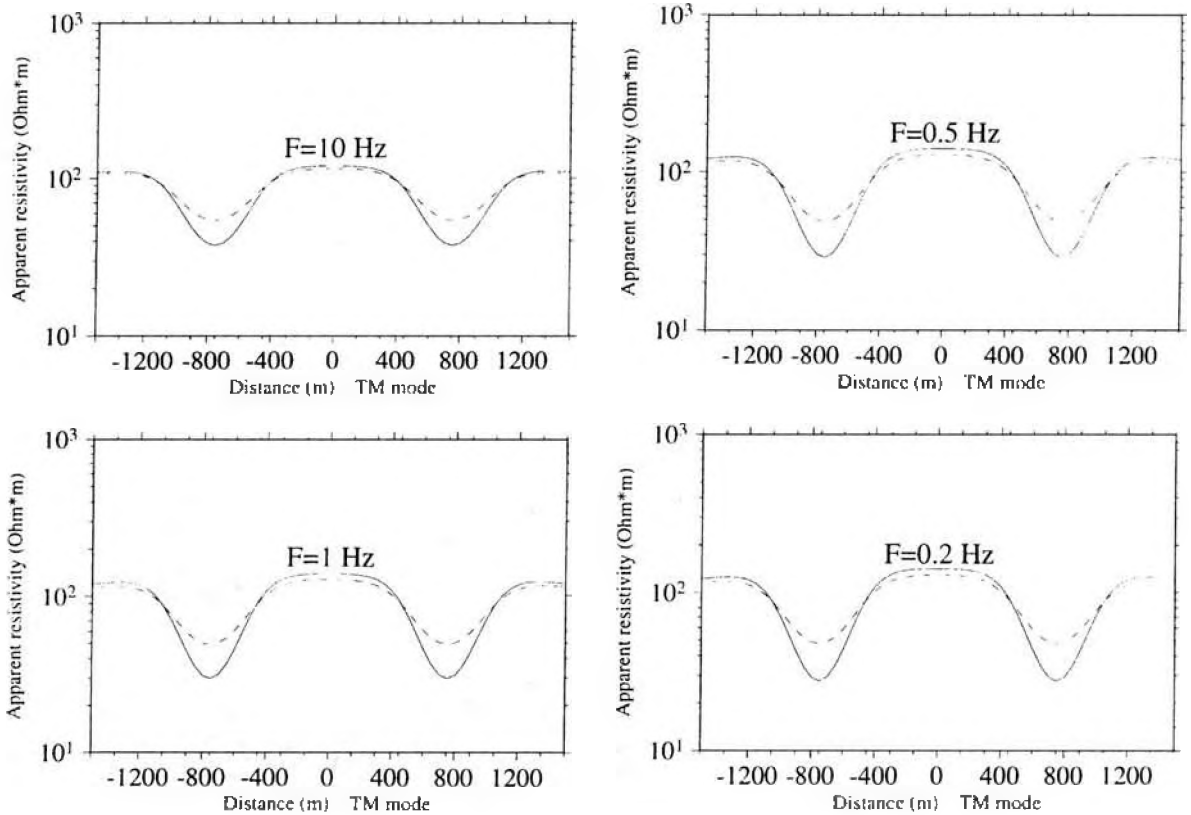

Figure 6. Numerical comparison of full IE solution (a), and QL approximation (b) computed for Model 2 (Fig. 5) at the frequencies 10, 1, 0.5, and 0.2 Hz. Calculations are performed for receivers located along profiles parallel to the y-axis on the surface. Plots present apparent resistivities computed for TM mode (ρ_{yx}).

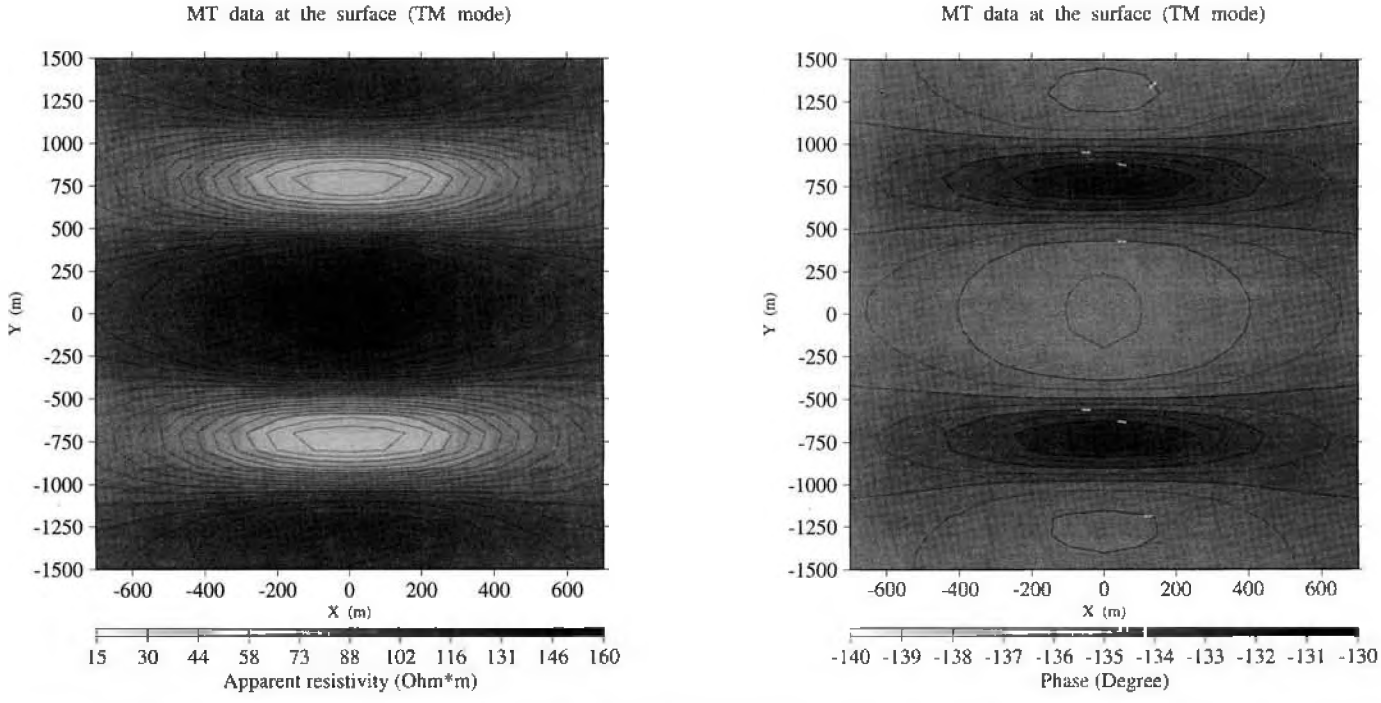

Figure 1. (a) Apparent resistivity amplitude distribution for the model shown in Fig. 5, calculated on the surface of the Earth for a frequency of 1 Hz. (b) Impedance phase distribution for the model shown in Fig. 5, calculated for a frequency of 1 Hz.

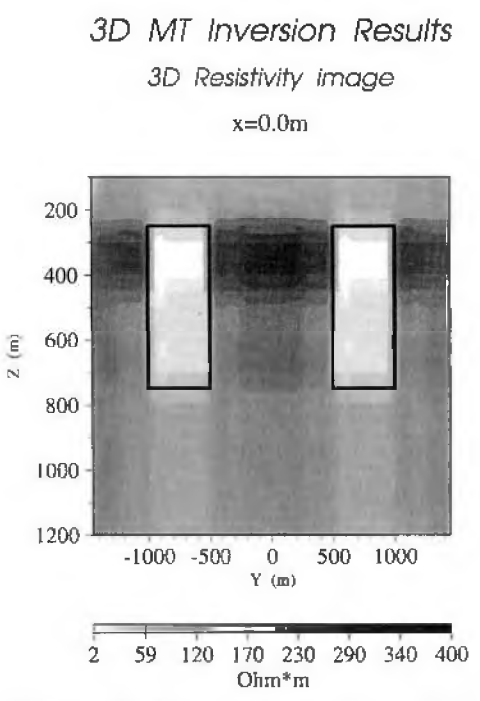

Figure 8. Vertical slice along the line $x = 0$ of the results of inversion of the data with 5% noise added for the model shown in Fig. 5.

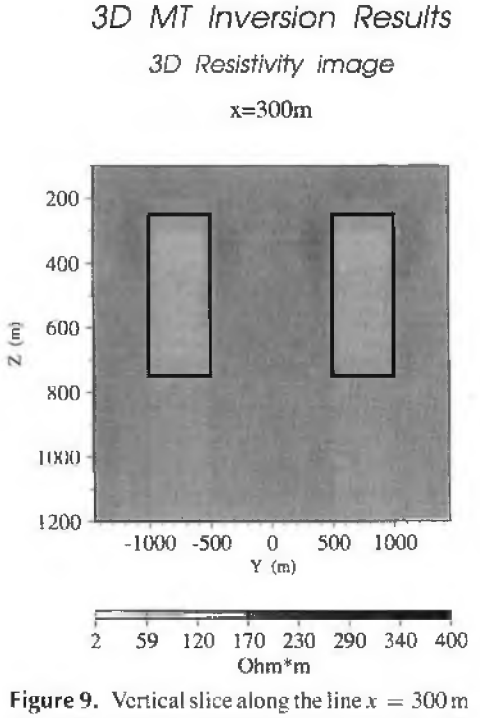

Figure 9. Vertical slice along the line $x = 300$ m of the results of inversion of the data with 5% noise added for the model shown in Fig. 5.

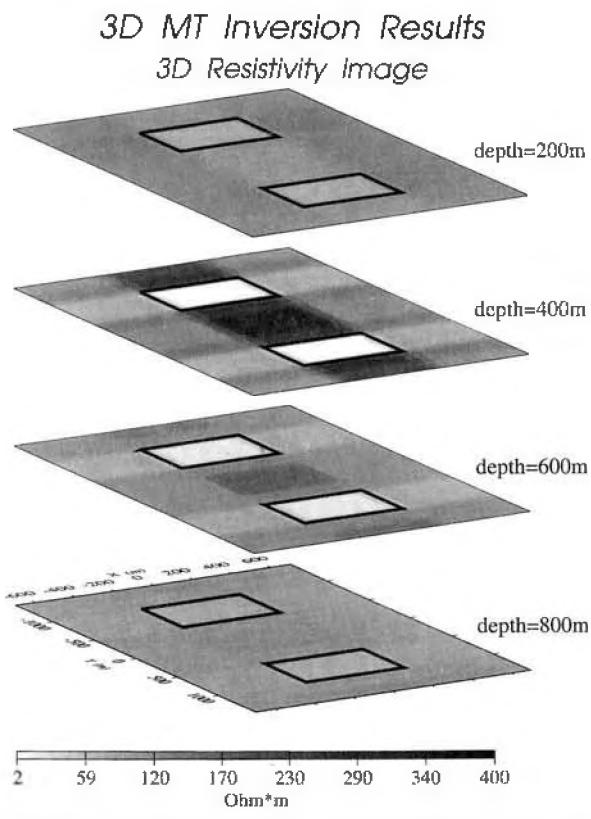

Figure 10. The volume image of the inverted model computed from EM data (with 5% noise added) collected along 15 profiles on the surface of the Earth for four frequencies (10, 1, 0.5, and 0.2 Hz) for the model shown in Fig. 5.

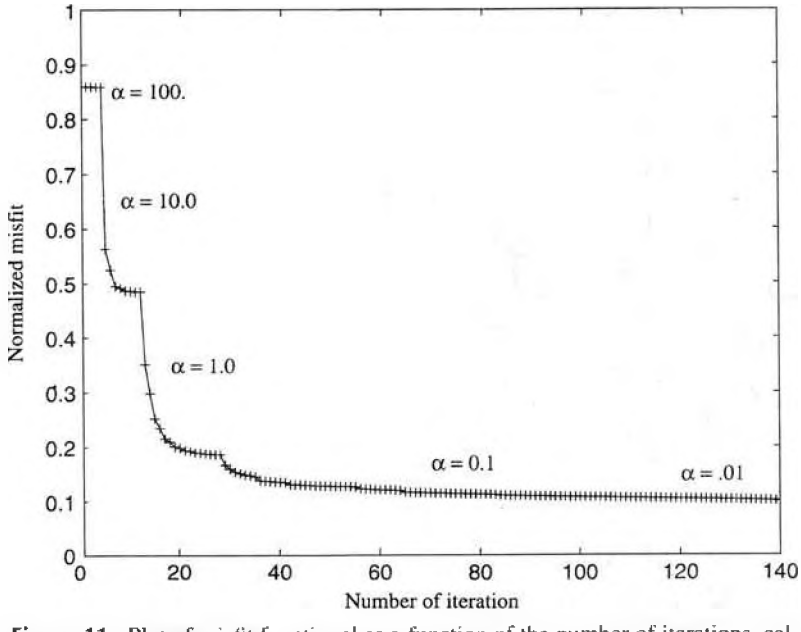

Figure 11. Plot of misfit functional as a function of the number of iterations, calculated during inversion.

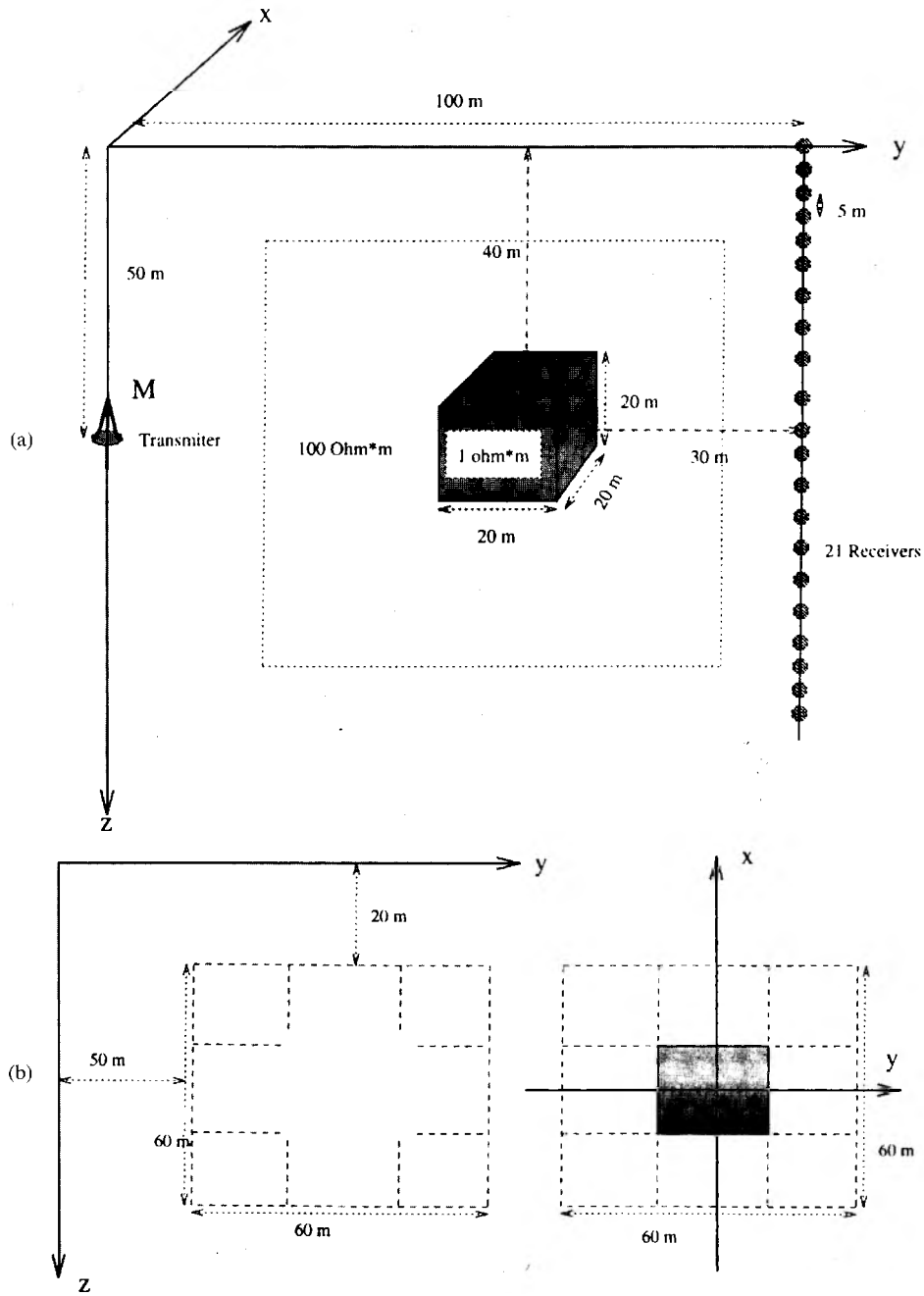

Figure 12. (a) Model of conducting body excited by the vertical dipole in the borehole (Model 3). (b) Inverse area is subdivided into 27 substructures; the size of the substructures is selected to be equal to the size of the actual conducting body.

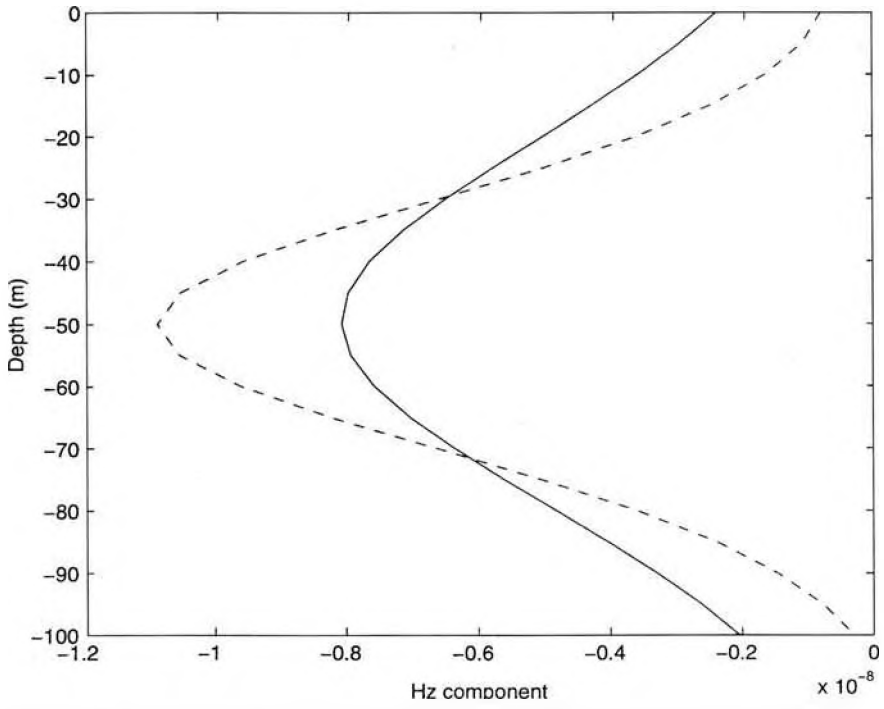

Figure 13. Plots of vertical anomalous magnetic field H_z^a (real and imaginary parts) calculated at the frequency 50 kHz along the borehole.

5.2 *Cross-borehole vertical magnetic dipole excitation model*

Let us consider a model simulating an orebody (Bertrand and McGaughey, 1994). We present the orebody as a cube with side 20 m and resistivity 1 ohm-m embedded in a homogeneous media with resistivity 100 ohm-m. This model simulates typical massive-sulfide deposits. The orebody is located exactly in the middle of the two boreholes at a depth of 40 m. The distance between the boreholes is 100 m (Fig. 12a). Cross-borehole EM surveys can be conducted by the frequency-domain vertical magnetic dipole system. The transmitter (vertical magnetic dipole) is located at a depth of 50 m in the first borehole, and 21 receivers, observing the vertical magnetic field, are in the second borehole, from a depth of 0 to 100 m. The plots of the vertical anomalous magnetic field H_z^a (real and imaginary parts) calculated for the frequency 50 kHz along the borehole are presented in Fig. 13.

The unknown region is subdivided into 27 substructures: The size of the substructures is selected to be equal to the size of the actual conducting body (Fig. 12b). The vertical slices of the geoelectrical model obtained as the result of the inversion for borehole data are presented at Fig. 14. Comparison of these results with the original model (Fig. 12a) shows that QL inversion produces a reasonable model of the target.

6 Conclusion

We have developed a fast algorithm for 3-D EM inversion based on the QL approximation of forward modeling. The method works for models with various sources of excitation, including plane waves for magnetotellurics, horizontal bipoles, vertical bipoles, horizontal rectangular loops, vertical magnetic dipoles, and the loop-loop system for surface (and airborne) electromagnetics.

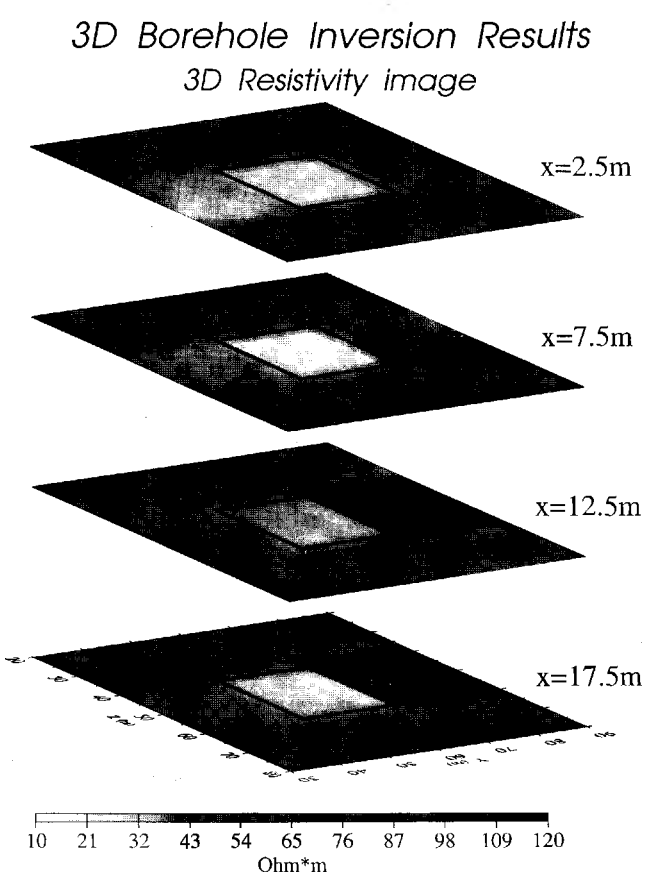

Figure 14. The vertical slices of the geoelectrical model (at the x positions 2.5 m, 7.5 m, 12.5 m, 17.5 m) obtained as the result of the inversion for one borehole profile vertical magnetic data, presented at Fig. 13. The size of the substructures is selected to be equal to the size of the actual conducting body (Fig. 12(b)).

The main advantage of the method is that it reduces the original nonlinear inverse problem to a set of linear inverse problems to obtain a rapid 3-D conductivity inversion. The QL inverse problem is solved by a regularized gradient-type method that ensures stability and rapid convergence.

Acknowledgments

The authors acknowledge the support of the University of Utah Consortium of Electromagnetic Modeling and Inversion (CEMI), which includes CRA Exploration Ltd., Newmont Exploration, Western Mining, Kennecott Exploration, Schlumberger-Doll Research, Shell Exploratie en Produktie Laboratorium, Western Atlas, the United States Geological Survey, Zonge Engineering, Mindeco, MIM Exploration, and BHP Exploration.

We thank Dr. Z. Xiong for providing the forward-modeling IE code and Dr. Michael Oristaglio and Dr. Carlos Torres-Verdin for their useful discussions which helped to improve the manuscript.

We also thank Weidong Li for his help with numerical calculations.

References

Born, M., 1933, *Optics*: Springer Pub. Co., Inc.

Berdichevsky, M. N., and Zhdanov, M. S., 1984, Advanced theory of deep geomagnetic sounding: Elsevier Science Publ. Co., Inc.

Bertrand, M. J., and McGaughey, J., 1994, Crosshole EM detectability of high-conductivity contrast anomalies: 64th Ann. Mt., Soc. Expl. Geophys. Expanded Abstracts, 407–410.

Druskin, V., and Knizhnerman, L., 1994, Spectral approach to solving three-dimensional Maxwell's diffusion equations in the time and frequency domains: Radio Sci., **29**, 937–953.

Eaton, P. A., 1989, 3-D electromagnetic inversion using integral equations: Geophys. Prosp., **37**, 407–426.

Gusarov, A. L., 1981, About the uniqueness of the solution of the magnetotelluric inverse problem, *in* Mathematical models in geophysical problems: Moscow Univ. Press, 31–80.

Habashy, T. M., Groom, R. W., and Spies, B. R., 1993, Beyond the Born and Rytov approximations: A nonlinear approach to EM scattering: J. Geophys. Res., **98**, 1759–1775.

Habashy, T. M., Oristaglio, M. L., and de Hoop, A. T., 1994, Simultaneous nonlinear reconstruction of two-dimensional permittivity and conductivity: Radio Sci., **29**, 1101–1118.

Hohmann., G. W., 1975, Three-dimensional induced polarization and EM modeling: Geophysics, **40**, 309–324.

Kleinman, R. E., and van den Berg, P. M., 1993, An extended range-modified gradient technique for profile inversion: Radio Sci., **28**, 877–884.

Madden, T. R., and Mackie, R. L., 1989, Three-dimensional magnetotelluric modeling and inversion: Proc. IEEE, **77**, 318–332.

Newman, G. A., and Alumbaugh, D. L., 1995, 3-D massively parallel electromagnetic inversion: PIERS Proc., Univ. of Washington, 324.

Smith, J .T., and Booker, J. R., 1991, Rapid inversion of two- and three-dimensional magnetotelluric data: J. Geophys. Res., **96**, 3905–3922.

Svetov, B. S., and Gubatenko, V. P., 1985, About the equivalence of the system of the extraneous electric and magnetic currents: Radiotechniques and electronics, No. 4, 31–40.

Tikhonov, A. N., and Arsenin, V. Y., 1977, Solution of ill-posed problems: W. H. Winston and Sons.

Torres-Verdín, C., and Habashy, T. M., 1994, Rapid 2.5-dimensional forward modeling and inversion via a new nonlinear scattering approximation: Radio Sci., **29**, 1051–1079.

———1995a, Two-steps linear inversion: Radio Sci., **29**, 1051–1079.

———1995b, An overview of the extended Born approximation as a nonlinear scattering approach, and its application to cross-well resistivity imaging: PIERS Proc., Univ. of Washington, 321.

Tripp, A. C., 1990, Group theoretic reduction of the EM impedance matrix for large-contrast symmetric prisms in a layered earth: Pageoph, **133**, 127–147.

Tripp, A. C., and Hohmann, G. W., 1993, Three-dimensional EM cross-well inversion: IEEE Trans. Geosci. Remote Sensing, **31**, 121–126.

Wannamaker, P. E., 1991, Advances in 3-D magnetotelluric modeling using integral equations: Geophysics, **56**, 1716–1728.

Weidelt, P., 1975, EM induction in three-dimensional structures: J. Geophys., **41**, 85–109.

Xie, G., and Lee, K. H., 1995, Nonlinear inversion of 3-D electromagnetic data: PIERS Proc., Univ. of Washington, 323.

Xiong, Z., 1992, EM modeling of three-dimensional structures by the method of system iteration using integral equations: Geophysics, **57**, 1556–1561.

Xiong, Z., and Kirsch, A., 1992, Three-dimensional earth conductivity inversion: J. Comput. Appl. Math., **42** , 109–121.

Xiong, Z., and Tripp, A. C., 1993, Scattering matrix evaluation using spatial symmetry in EM modeling: Geophys. J. Internat., **114**, 459–464.

Zhdanov, M. S., 1993, Tutorial: Regularization in inversion theory: Colorado School of Mines.

Zhdanov, M. S., and Chernyak, V. V., 1987, An automated method of solving the two-dimensional inverse problem of electromagnetic induction within the earth: Trans. (Doklady) USSR Acad. Sci., Earth Sci., **296**, 59–63.

Zhdanov, M. S., and Keller, G., 1994, The geoelectrical methods in geophysical exploration: Elsevier Science Pub. Co., Inc.

Zhdanov, M. S., and Fang, S., 1996a, Quasi-linear approximation in 3-D EM modeling: Geophysics, **61**, 646–665.

———1996b, Three-Dimensional quasi-linear electromagnetic inversion: Radio Sci., **31**(4), 741–754.

Appendix: Regularized steepest-descent method for minimizing the parametric functional

To get a stable solution of Eqs. (28) and (31), we introduced the parametric functional:

$$P^{\alpha}(\mathbf{m}) = \phi(\mathbf{m}) + \alpha\, S(\mathbf{m}),$$

where functionals $\phi(\mathbf{m})$ and $S(\mathbf{m})$ were determined by Eqs. (36) and (37). To solve the minimization problem (40) we calculate the first variation of the parametric functional under the assumption that $\Delta\tilde{\sigma}$ and λ are, temporarily, constants:

$$\delta P^{\alpha}(\mathbf{m}) = 2\,\mathrm{Re}\,\{\delta\mathbf{m}^{*}[\underline{\mathbf{G}}^{F*}(\underline{\mathbf{G}}^{F}\mathbf{m} - \mathbf{F}) + [\mathbf{m} - (\underline{\mathbf{I}} + \underline{\Lambda})\Delta\sigma] + \alpha(\mathbf{m} - \mathbf{m}_{p})]\}.$$

Let us select $\delta\mathbf{m}$ as

$$\delta\mathbf{m} = -k^{\alpha}\,\ell^{\alpha}(\mathbf{m}), \quad 0 < k^{\alpha} < \infty, \tag{A1}$$

where

$$\ell^{\alpha}(\mathbf{m}) = \underline{\mathbf{G}}^{F*}(\underline{\mathbf{G}}^{F}\mathbf{m} - \mathbf{F}) + [\mathbf{m} - (\underline{\mathbf{I}} + \underline{\Lambda})\Delta\sigma] + \alpha\,(\mathbf{m} - \mathbf{m}_{p}). \tag{A2}$$

This selection makes $\delta P^{\alpha}(\mathbf{m}) = -2\,k^{\alpha}\,\mathrm{Re}\{\ell^{\alpha *}(\mathbf{m})\,\ell^{\alpha}(\mathbf{m})\} < 0$. That means that the parametric functional is reduced if we apply perturbation (A1) to the model parameters. We construct an iteration process as follows:

$$\mathbf{m}^{\alpha}_{N+1} = \mathbf{m}^{\alpha}_{N} + \delta\mathbf{m}_{N} = \mathbf{m}^{\alpha}_{N} - k^{\alpha}_{N}\,\ell^{\alpha}(\mathbf{m}_{N}), \tag{A3}$$

where

$$\ell^{\alpha}(\mathbf{m}_{N}) = \underline{\mathbf{G}}^{F*}(\underline{\mathbf{G}}^{F}\mathbf{m}_{N} - \mathbf{F}) + [\mathbf{m}_{N} - (\underline{\mathbf{I}} + \underline{\Lambda}_{N})\Delta\sigma_{N-1}] + \alpha\,(\mathbf{m}_{N} - \mathbf{m}_{p}). \tag{A4}$$

The reflectivity $\boldsymbol{\lambda}_N$ is determined from m_N using Eq. (31):

$$\underline{\mathbf{E}}^n \boldsymbol{\lambda}_N = \underline{\mathbf{G}}^E \mathbf{m}_N, \tag{A5}$$

Note that the anomalous conductivity has to satisfy the condition (componentwise)

$$\mathrm{Re}(\Delta\tilde{\boldsymbol{\sigma}}_{N-1}) \geq -\sigma_n; \quad \mathrm{Im}(\Delta\boldsymbol{\sigma}_{N-1}) \leq \omega\varepsilon_n \tag{A6}$$

because the electrical conductivity and dielectric permittivity have to be positive. Therefore, the conductivity $\Delta\tilde{\boldsymbol{\sigma}}_{N-1}$ can be found by using Eqs. (33) and (A6) with the following conditions (componentwise):

$$\begin{aligned}\mathrm{Re}(\Delta\tilde{\sigma}_{N-1}) &= \mathrm{Re}\left[\sum_{\omega}[(1+\lambda_{N-1})^*(1+\lambda_{N-1})]\right]^{-1}\left[\sum_{\omega}(1+\lambda_{N-1})^* m_{N-1}\right] \\ &= a_{N-1} \quad \text{for } a_{N-1} \geq -\sigma_n\end{aligned} \tag{A7}$$

and

$$\mathrm{Re}(\Delta\tilde{\sigma}_{N-1}) = -\tfrac{1}{2}\sigma_n, \quad \text{for } \mathbf{a}_{N-1} \leq -\sigma_n. \tag{A8}$$

Similarly,

$$\begin{aligned}\mathrm{Im}(\Delta\tilde{\sigma}_{N-1}) = -\omega\,\mathrm{Im}\left\{\left[\sum_{\omega}\omega(1+\lambda_{N-1})^*(1+\lambda_{N-1})\right]^{-1}\right. \\ \left.\times\left[\sum_{\omega}(1+\lambda_{N-1})^* m_{N-1}\right]\right\} = b_{N-1},\end{aligned}$$

$$\text{for } b_{N-1} < \omega\varepsilon_n$$

$$\mathrm{Im}(\Delta\tilde{\sigma}_{N-1}) = \tfrac{1}{2}\omega\varepsilon_n, \quad \text{for } b_{N-1} \geq \omega\varepsilon_n.$$

The initial iteration should be done using the formula

$$\mathbf{m}_1^\alpha = \mathbf{m}_0^\alpha + \delta\mathbf{m}_0 = \mathbf{m}_0^\alpha - k_0^\alpha\,[\underline{\mathbf{G}}^{F*}(\underline{\mathbf{G}}^F \mathbf{m}_p - \mathbf{F})], \tag{A9}$$

where

$$\mathbf{m}_p = (\underline{\mathbf{I}} + \underline{\boldsymbol{\Lambda}}_p)\Delta\boldsymbol{\sigma}_p$$

The second iteration is

$$\mathbf{m}_2^\alpha = \mathbf{m}_1^\alpha + \delta\mathbf{m}_1 = \mathbf{m}_1^\alpha - k_1^\alpha\,\ell^\alpha(\mathbf{m}_1), \tag{A10}$$

where

$$\ell^\alpha(\mathbf{m}_1) = \underline{\mathbf{G}}^{F*}(\underline{\mathbf{G}}^F \mathbf{m}_1 - \mathbf{F}) + [\mathbf{m}_1 - (\underline{\mathbf{I}} + \underline{\boldsymbol{\Lambda}}_1)\Delta\boldsymbol{\sigma}_p] + \alpha\,(\mathbf{m}_1 - \mathbf{m}_p). \tag{A11}$$

The coefficient k_n^α can be determined from the condition

$$P^\alpha(\mathbf{m}_{N+1}^\alpha) = P^\alpha\left[\mathbf{m}_N^\alpha - k_N^\alpha\,\ell^\alpha(\mathbf{m}_N)\right] = f(k_N^\alpha) = \min!$$

Solution of this minimization problem gives the following best estimation for the length of the step:

$$k_N^\alpha = \frac{\ell^{\alpha*}(\mathbf{m}_N^\alpha)\ell^\alpha(\mathbf{m}_N^\alpha)}{\ell^{\alpha*}(\mathbf{m}_N^\alpha)(\underline{\mathbf{G}}^{F*}\underline{\mathbf{G}}^F + \alpha\underline{\mathbf{I}})\ell^\alpha(\mathbf{m}_N^\alpha)}. \tag{A12}$$

Using Eqs. (A2), (A3), and (A12), we can obtain $\mathbf{m}$ iteratively.